

# Longitudinal flow decorrelations in small collision systems

Hadi Mehrabpour<sup>1,2,\*</sup> and Abhisek Saha<sup>1,2,†</sup>

<sup>1</sup>*School of Physics, Peking University, Beijing 100871, China*

<sup>2</sup>*Center for High Energy Physics, Peking University, Beijing 100871, China*

This study presents a detailed analysis of longitudinal flow decorrelations in light ion collisions at both Relativistic Heavy Ion Collider (RHIC) and Large Hadron Collider (LHC) energies, focusing on various *ab-initio* models of oxygen structure. We identify that the correlator  $V_{2\Delta}$  effectively differentiates between the variational Monte Carlo (VMC) structure and other models, such as Nuclear Lattice Effective Field Theory (NLEFT) and the Projected Generator Coordinate Method (PGCM), revealing similar behaviors between the latter two. By utilizing the isolated non-spherical components, we highlight significant negative contributions in the structure generated by VMC compared to the other configurations. Additionally, we show that employing decorrelation  $r_2$  to mitigate non-flow effects proves beneficial in identifying various modeled structures. We further examine flow decorrelations across different systems, including d+Au and O+O collisions at 200 GeV, as well as Ne+Ne and O+O collisions at 6.37 TeV, indicating a hierarchy in decorrelations that underscores the complexity of these interactions. Our findings emphasize that the role of asymmetry in d+Au collisions and its impact on flow correlations is mitigated by the correlator  $V_{2\Delta}(\eta, \eta_{\text{ref}})$ . Additionally, our analysis of flow angle decorrelations shows diverse distributions of  $\cos(2\Delta\psi_2)$  vs. overall flow magnitude in d+Au collisions compared to those in other collision systems, as indicated by the mean value of  $\cos(2\Delta\psi_2)$ .

## I. INTRODUCTION

The study of nuclear structure has long been a cornerstone of nuclear physics, providing insights into the fundamental forces and interactions that govern matter at the subatomic level [1]. Investigating nuclear structure in relation to the complex nucleon-nucleon interactions presents a significant challenge in low-energy nuclear physics [2, 3], driving research into various phenomenological models [3–7] and experimental methodologies [8–10]. This complexity has been explored through advanced models, including NLEFT simulations [11, 12], PGCM [13–15], and VMC [16], particularly for nuclei such as oxygen and neon. The effort of low-energy experiments is complemented by exploring nuclear structure in ultra-relativistic ion collisions [17]. These studies utilize nucleon distribution data obtained from various models.

The matter distribution in colliding nuclei is revealed through the shape and size of the energy density in the overlap region [18–20]. The initial shape of energy deposition depends on both the collision geometry and quantum fluctuations in nuclear wavefunctions [21], which lead to event-by-event fluctuations [22, 23]. It is well-established that the initial state properties are analyzed through collective flow obtained from the spectra of emitted particles [24–26]. Since flow is sensitive to matter distribution in nuclei [27–34], it serves as a suitable observable for studying nuclear structures. Recently, a number of studies have been conducted to investigate light nuclear structures, particularly  $^{16}\text{O}$  and  $^{20}\text{Ne}$ , which may pave the way for discoveries in high-energy experiments

[17]. In Ref.[35], the NLEFT model has been utilized to generate the oxygen nucleonic configurations. The findings indicate that the O+O collision commence in a state that is significantly out of equilibrium, and it has been observed that at the LHC and RHIC, these collisions only reach a hydrodynamic regime after considerable time has elapsed. The first measurements of azimuthal anisotropies in O+O collisions for the collected data at RHIC have been done in Ref.[36]. The consistency of VMC with experimental data has been observed. Moreover, *ab-initio* nucleon-nucleon correlations (VMC, NLEFT, PGCM) and their impact on O+O collisions have been studied at RHIC energies [37]. A large deviation of elliptic flow for VMC from NLEFT and PGCM has been observed in central collisions. Since the advanced models are able to address the emergence of the clustering correlations in light nuclei, Refs.[38, 39] have explored the effects of  $\alpha$ -clustering in the relativistic O+O collisions. Comparing of  $^{16}\text{O}$  structure with  $^{20}\text{Ne}$  structure has been done in symmetric and asymmetric collisions [40, 41]. The bowling pin shape of Ne in comparison with oxygen structures has been studied.

Regarding the rapid expansion of the fireball due to the presence of strong pressure gradients, information about initial fluctuations is also encoded in the longitudinal direction [42–48]. Investigations utilizing models to analyze two-particle correlations as a function of pseudorapidity have uncovered significant event-by-event fluctuations in both the magnitude and phase of the flow. This is particularly evident between two distinct pseudorapidities, leading to notable discrepancies such that  $v_n(\eta_a)$  differs from  $v_n(\eta_b)$ , indicative of forward-backward asymmetry, and  $\psi_n(\eta_a)$  varies from  $\psi_n(\eta_b)$ , reflecting a twisting of the event plane [42, 49, 50]. Recently, flow decorrelations have been analyzed in collisions involving heavy nuclei of similar masses but different structures [51] using a dy-

\* mehrabpour@pku.edu.cn

† saha@pku.edu.cn

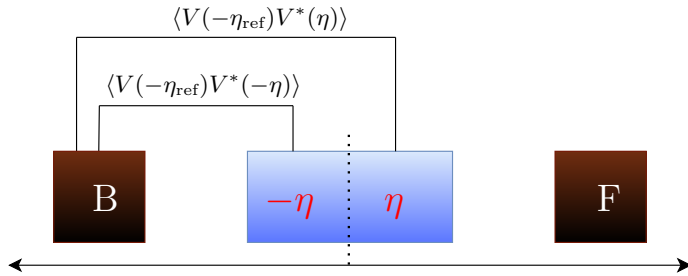


FIG. 1. Schematic of longitudinal or beam direction is illustrated here. It shows using pseudorapidity bins in definitions of longitudinal decorrelations.

namical transport model. By reducing the impact of non-flow effects, it has been found that while non-spherical structures considerably increase the overall flow magnitude  $v_2$ , they do not change its longitudinal profile.

To present a comprehensive study of small systems, investigation of light nuclear structure in the longitudinal direction is required. The aim of this paper is to investigate the patterns defined in Ref.[51] for the recently proposed small collision systems O+O and Ne+Ne, as well as d+Au. In Section II, we provide a brief overview of the materials required for this analysis. Section III A investigates the effects of advanced models on observables through various configurations of oxygen. Within this section, we focus on the differences arising from spherical oxygen configurations by isolating the deformation components. Additionally, we emphasize that the slope parameter can serve as an effective discriminator for studying nuclear structures. In Section III B, we conduct a comparative analysis of O+O collisions and d+Au collisions to explore nuclear structures at different scales within the context of RHIC energy. We also present predictions regarding longitudinal decorrelation for O+O and Ne+Ne collisions in anticipation of the upcoming LHC Run. The findings are summarized in the concluding section.

## II. MATERIALS

In the study of high-energy nuclear collisions, the concept of flow is pivotal for understanding the azimuthal distribution of emitted particles [24–26]. Flow can be quantitatively described using harmonic coefficients, specifically through the notation  $V_n = v_n e^{i2\psi_n}$  [52–54], where  $v_n$  represents the magnitude of harmonic flows and  $\psi_n$  denotes the event-plane angle associated with them. Here, the investigation focuses on elliptic flow  $V_2$ , which reflects the hydrodynamic response to the elliptically-shaped overlap region and its associated quadrupole deformations. Nevertheless, it is crucial to recognize that the flow vector  $V_2$  cannot be derived from isolated events [55]. Rather, we drive rotationally invari-

ant combinations of flow vectors by analyzing the moments of the associated  $q_2$  vectors within a defined region of phase space  $\eta_a$ :  $q_2(\eta_a) = \frac{1}{N} \sum_{k \in \eta_a} e^{i2\phi_k}$  [54, 56], where the sum is performed over all  $N$  hadrons located within the specified phase space region  $\eta_a$ , and  $\phi_k$  represents the azimuthal angles of these particles [57]. The event average of the  $q_2$  vector moments acts as an estimator for the corresponding moments of the flow vectors:  $V_{2\Delta}(\eta_a, \eta_b) \equiv \langle V_2(\eta_a) V_2^*(\eta_b) \rangle = \langle q_2(\eta_a) q_2^*(\eta_b) \rangle$ , where the angular brackets denote an average taken over multiple events [58]. The moments  $V_{2\Delta}(\eta_a, \eta_b)$  reflect the phenomenon of factorization breaking in collective flow<sup>1</sup>[42]. This indicates that flow moments derived from different phase space regions  $\eta_a$  and  $\eta_b$  is the following [42, 59]:

$$V_{2\Delta}(\eta_a, \eta_b) = \frac{1}{N_{events}} \sum_{events} \frac{1}{N_a N_b} \sum_{k \in \eta_a, j \in \eta_b} e^{i2(\phi_k - \phi_j)}. \quad (1)$$

In contrast, the formula for flow moments calculated within a single region is represented as follows:

$$v_2(\eta_a) = \frac{1}{N_{events}} \sum_{events} \frac{1}{N_a(N_a - 1)} \sum_{k \neq j \in \eta_a} e^{i2(\phi_k - \phi_j)}.$$

To measure the extent of decorrelation between flow vectors in two distinct regions of phase space, we utilize the decorrelation coefficient [60–63]:

$$R(\eta_a, \eta_b) = \frac{V_{2\Delta}(\eta_a, \eta_b)}{\sqrt{v_2(\eta_a) v_2(\eta_b)}}. \quad (2)$$

In scenarios where multiparticle correlations are primarily influenced by flow, we find that  $R(\eta_a, \eta_b) < 1$ . This correlation coefficient serves as a valuable measure of flow decorrelation across different pseudorapidity bins [42].

The decorrelation observed in pseudorapidity is significantly affected by non-flow effects [60]. To tackle this issue, a modified factorization breaking coefficient has been introduced, defined as a ratio of two flow vector covariances derived from different pairs of bins [60, 64–68]:

$$r_{2;V}(\eta) = \frac{V_{2\Delta}(\eta, -\eta_{ref})}{V_{2\Delta}(-\eta, -\eta_{ref})}, \quad (3)$$

$$r_{2;\psi}(\eta) = \frac{\langle \cos(2\psi_2(\eta) - 2\psi_2(-\eta_{ref})) \rangle}{\langle \cos(2\psi_2(-\eta) - 2\psi_2(-\eta_{ref})) \rangle}. \quad (4)$$

In this context,  $\eta_{ref}$  acts as a common reference pseudorapidity, as illustrated in Fig.1. Experimental results indicate that decorrelation described by Eqs.3 and 4 can be qualitatively replicated by hydrodynamic and cascade models [60, 61]. This provides a robust framework for elucidating these indicated phenomena in high-energy nuclear collisions.

<sup>1</sup> Factorization breaking not only predicts a deviation from unity in the correlation coefficient between two flow vectors measured in separate pseudorapidity region, but it also encompasses this prediction between two bins of transverse momentum.

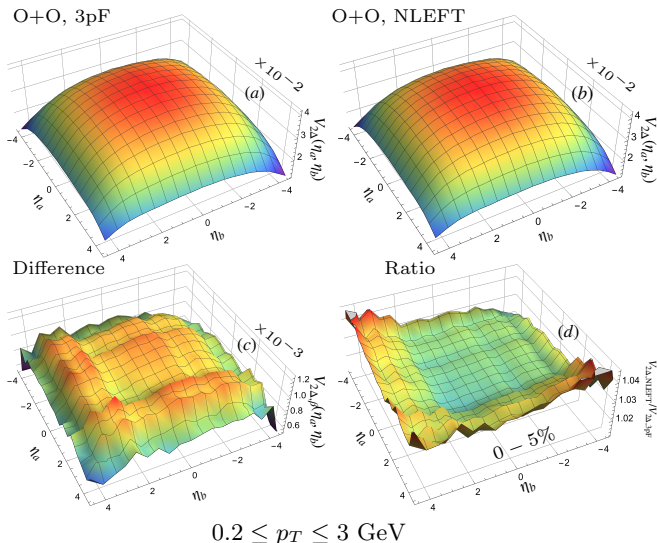


FIG. 2. Two-dimensional elliptic flow distribution  $V_{2\Delta}(\eta_a, \eta_b)$  is demonstrated for 3pF (a) and NLEFT (b) in 0 – 5% centrality at 200 GeV. Since we find the same presence of different models we just showed one model here. To isolate the deformation term the difference  $V_{2\Delta, \beta}(\eta_a, \eta_b) = V_{2\Delta, \text{NLEFT}} - V_{2\Delta, \text{3pF}}$  is displayed in (c). To discriminate of different oxygen structures, correlator  $V_2(\eta_a, \eta_b)$  is computed for NLEFT simulation normalized by  $V_{2\Delta, \text{3pF}}$  in panel (d).

In the following sections, we explore longitudinal decorrelations in small systems at RHIC and LHC energy collisions. To achieve this, we employ a combination of the 3D-Glauber Monte-Carlo model [69], (3+1)D viscous hydrodynamics (MUSIC)[70], and UrQMD [71] to generate 10000 fluctuating events for each type of collisions: d+Au and O+O at 200 GeV, as well as O+O and Ne+Ne at 6.37 TeV in preparation for the upcoming LHC Run. We consider 2000 oversampled events derived from the same hydrodynamic event, and then they are combined in the hadronic flow analysis. It is important to note that we have fixed the centrality range at 0 – 5%, where the maximum quadrupole deformation is anticipated, and we have selected a transverse-momentum range of  $0.2 \leq p_T \leq 3$  GeV to enhance our statistical sample.

### III. RESULTS

In this section, we elucidate the findings for O+O collisions at 200 GeV, highlighting the inherent nuclear characteristics as captured by three distinct models: NLEFT, PGCM, and VMC (Sec.III A). We undertake a comparative analysis of O+O and d+Au collisions to investigate the influence of system size and nuclear configurations in Sec.III B. Furthermore, we extend this methodology to examine O+O and Ne+Ne collisions within the framework of the NLEFT model, offering predictions for forthcoming LHC Runs.

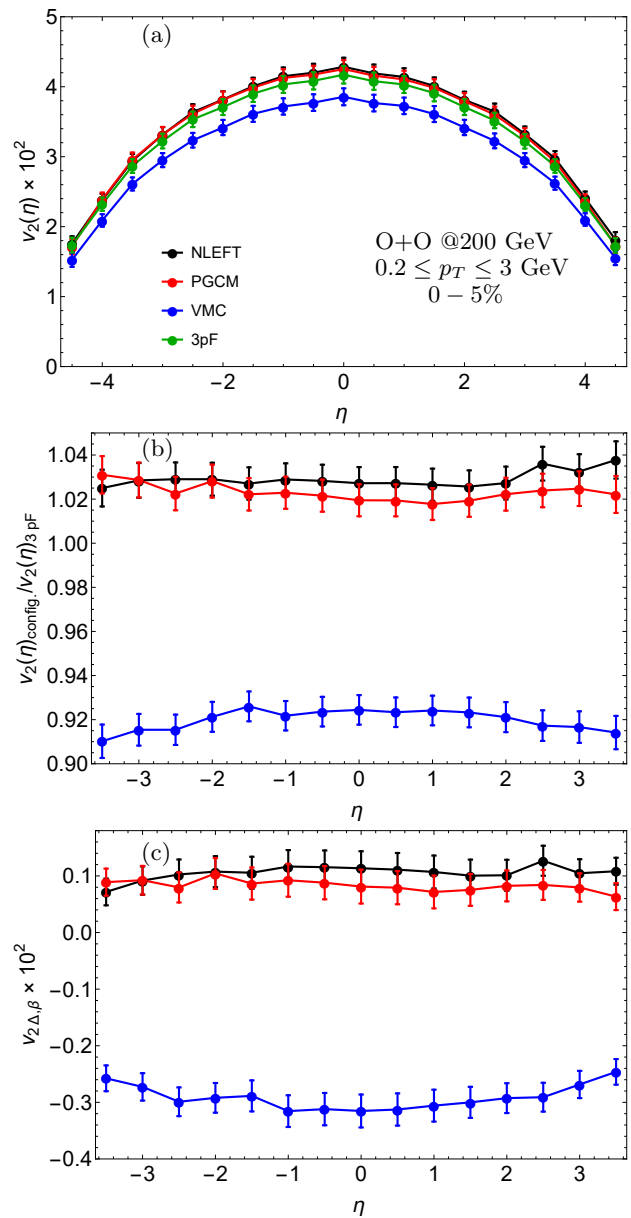


FIG. 3. (a) The diagonal terms of  $V_{2\Delta}(\eta_a, \eta_b)$ ,  $v_2(\eta)$ , in Fig.2 are demonstrated for different *ab-initio* models. (b) Also the ratio  $v_{2, \text{config}}/v_{2, \text{3pF}}$  are computed for different oxygen structures. This ratio plays the role of a structure discriminator. The deformation contributions in each oxygen structure are displayed in (c).

#### A. Discriminators of Oxygen Structures

Recently, several studies have been conducted to predict bulk observables of  $^{16}\text{O}$  using advanced *ab-initio* models [36–38, 40, 41, 72]. These include: 1) NLEFT simulations utilizing a minimal pion-less EFT Hamiltonian [11, 12], 2) VMC simulations grounded on  $\text{N}^2\text{LO}$  chiral EFT Hamiltonian [16], and 3) PGCM calculations related to  $\text{N}^3\text{LO}$  chiral EFT Hamiltonian [13–15]. The different Hamiltonians and approximations employed re-

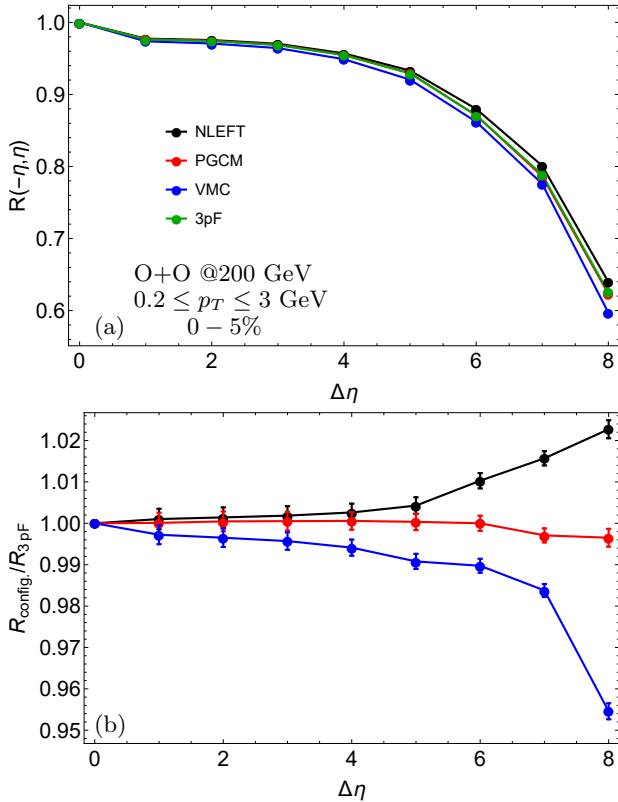


FIG. 4. Decorrelations of two pseudorapidity intervals at  $\pm\eta$  in panel (a) and ratios (configs/3pF) to determine the different oxygen structures in panel (b) are presented. The results indicate that this correlator cannot identify PGCM from spherical shape of  $^{16}\text{O}$  (3pF).

sult in varied tetrahedral-like clustering correlations [38], which consequently lead to diverse predictions regarding observables of relativistic O+O collisions. Although multiple studies have been conducted using these models, recent STAR results shows that only the observables derived from VMC configurations show better alignment with RHIC data in the mid-rapidity region [36]. The distinctions between VMC and other models have been discussed in Ref.[37].

In this section, we study different oxygen structures, NLEFT, PGCM and VMC, to give a prediction of longitudinal observables. Also, we compare these models with the spherical structure of oxygen generated by the charge density 3pF parametrization of the nucleus. It should be noted that we considered  $R = 2.608$  fm,  $a_0 = 0.513$  fm, and  $w = -0.051$  to generate the charge density of spherical oxygen [37]. The information of flow decorrelations is encoded in the two-dimensional distribution of  $V_{2\Delta}(\eta_a, \eta_b)$  which is found by the 2-particle correlation (2PC) method [73] in Eq.1. Fig.2a and Fig.2b display the distributions obtained by 3pF and NLEFT densities respectively in 0 – 5% central O+O collisions at 200 GeV center-of-mass energy. The same effect is observed

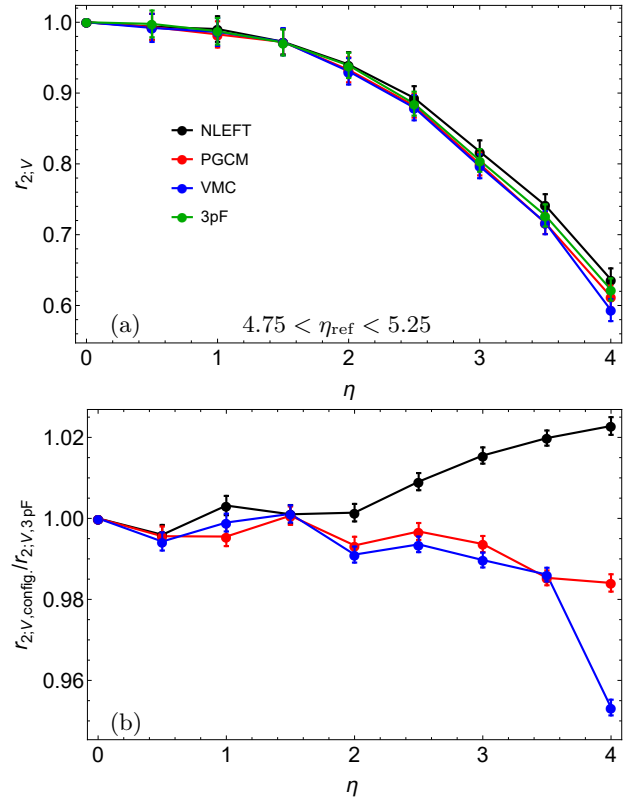


FIG. 5. Correlators  $r_{2;V}$  (a) for NLEFT (black), PGCM (red), VMC (blue), and spherical shape of oxygen (green). Also, discriminations of the modern models are presented in panel (b) using the ratio  $r_{2;V,\text{configs.}}/r_{2;V,3\text{pF}}$ .

for these structures on flow decorrelations<sup>2</sup>. The flow decorrelation of Eq.1 includes independent contributions of spherical, deformed and non-flow effects such as  $V_{2\Delta} = V_{2\Delta,sp} + V_{2\Delta,\beta} + \delta_{nf}$  [51]. Since the shape of the colliding nuclei also impacts the elliptic flow [18, 19, 74–76] and its longitudinal structure [77], we understood these effects by studying deformation term. The deformation part is isolated by subtracting of  $V_{2\Delta,\text{NLEFT}} - V_{2\Delta,3\text{pF}}$  [51]. The result of this difference is depicted in Fig.2c. As can be seen, deformation part is  $\approx 10^{-3}$ , one order of magnitude smaller. Normalizing  $V_{2\Delta,\text{NLEFT}}/V_{2\Delta,3\text{pF}}$  gives the information about an independent sampling of nucleons from NLEFT or existing of a  $NN$  correlations. Fig.2d shows the deviation of this ratio from unity which implies the presence of  $NN$  correlations in the NLEFT Hamiltonian.

To investigate the different oxygen structures, we study diagonal ridges of  $V_{2\Delta}(\eta_a, \eta_b)_{\text{configs}}$  along  $\eta = (\eta_a + \eta_b)/2$  illustrated in Fig.3a. It can be seen that decreasing of amplitudes are similar in positive and negative  $\eta$  regions. Comparing of normalized configurations are also depicted

<sup>2</sup> We also checked PGCM and VMC, and then we found the same behavior.

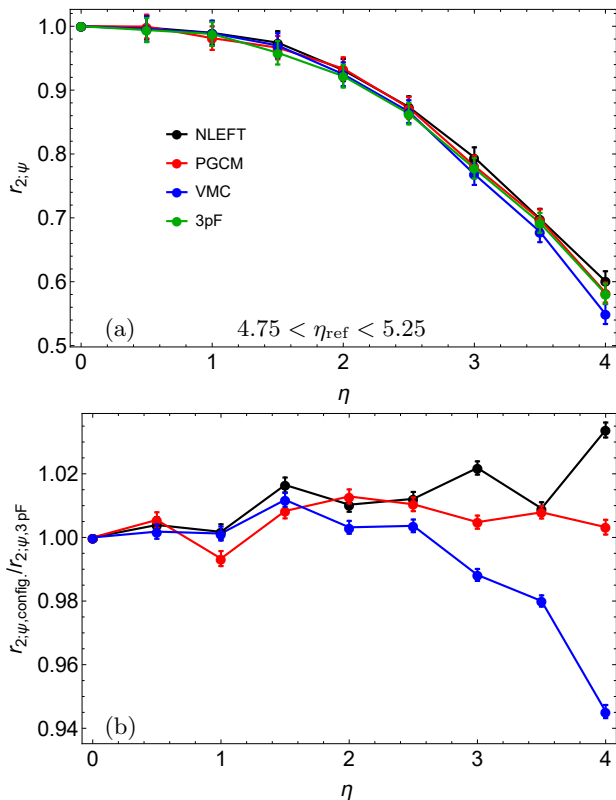


FIG. 6. Similar to Fig.5 for flow angle decorrelations  $r_{2,\psi}$ .

in Fig.3b. Due to different encoding structure properties of models, the behavior of  $v_2(\eta)$  obtained by VMC configurations is differed up to 10% from NLEFT and PGCM configurations. Moreover, the deviation from spherical structure is  $\approx 3\%$  for NLEFT (and PGCM) and  $\approx 9\%$  for VMC. These results is qualitatively consistent with the calculations in Ref.[37]. Furthermore, the results of deformation contributions in each structure are shown in Fig.3c. The PGCM and NLEFT deformation contributions are the same and positive, while flow decorrelation for VMC structure has negative and larger deformation term such that  $v_{2\Delta,\beta}(\text{VMC}) \approx -2.5v_{2\Delta,\beta}(\text{NLEFT or PGCM})$ .

The degree of decorrelations manifests as deviation of the factorization  $R(\eta_a, \eta_b)$  from unity. This quantity is strongly influenced by non-flow effect correlations [60]. However, it measures isolated decorrelations of flow from its  $\eta$  dependence. Fig.4a shows forward-backward decorrelations  $R(-\eta, \eta)$  for different  $^{16}\text{O}$  structure collisions in most central. It can be seen for  $\Delta\eta > 3$  the decorrelations are started to increase significantly. However, the behaviors of decorrelations are the same for different models. By renormalizing  $R(-\eta, \eta)_{\text{configs}}$  with spherical one,  $R(-\eta, \eta)_{3pF}$ , the splitting of different structures is appeared. Fig.4b indicates that features of VMC are distinguishable from other two models such that they are 1% for  $\Delta\eta < 4$ , and 5% with PGCM and 7% with NLEFT in  $\Delta\eta = 8$ . Also, it indicates a separation between NLEFT

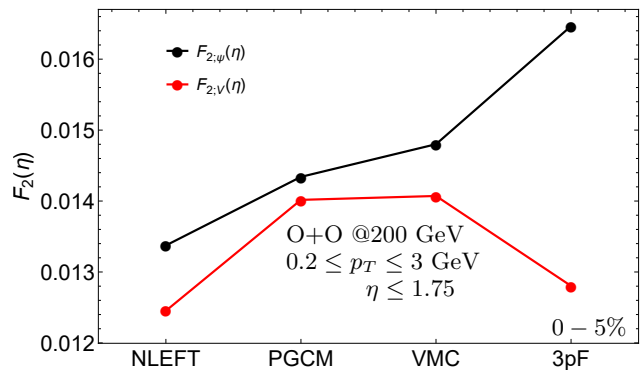


FIG. 7. The values of slope parameters  $F_{2,\psi}$  (black) and  $F_{2,V}$  (red) has been shown. As it is expected  $F_{2,\psi} > F_{2,V}$  due to  $r_{2,\psi} < r_{2,V}$ . These values are found in  $\eta \le 1.75$  where the correlators are almost linear.

and PGCM in  $\Delta\eta > 4$ , although the maximum difference is up to 2% in  $\Delta\eta = 8$ . Reducing non-flow contributions can be done using the correlators,  $r_{2,V}$  and  $r_{2,\psi}$ , defined in Eqs.3 and 4. Figs.5 and 6 present the results of the 3-pseudorapidity bin correlator of flow vector  $V_2$  and orientation  $\psi_2$ , respectively. In our simulations, we take the reference bin as  $4.75 < \eta_{ref} < 5.25$  far in the backward pseudorapidity region. We also symmetrize between the forward and backward pseudorapidities,

$$r_{2,V}(\eta) = \frac{1}{2} \left( \frac{V_{2\Delta}(\eta, -\eta_{ref})}{V_{2\Delta}(-\eta, -\eta_{ref})} + \frac{V_{2\Delta}(-\eta, \eta_{ref})}{V_{2\Delta}(\eta, \eta_{ref})} \right),$$

to increase statistics, which can be done for collisions of identical nuclei. The angle decorrelation can be symmetrized in a similar way. The results indicate same behavior for different structures in Fig.5a and Fig.6a. However, we differentiate between models using the ratio of  $r_{2,configs}/r_{2,3pF}$  in panels (b). It can be observed that  $r_{2,V}$  separates NLEFT from PGCM and VMC models in Fig.5b. This separation would be stronger by choosing a bin close to  $\eta_{ref}$  where the non-flow is increasing. The observable  $r_{2,\psi}$  distinguishes VMC from NLEFT and PGCM models, similar to  $R(-\eta, \eta)$ , as shown in Fig.6b. In contrast, the correlator  $r_{2,V}$  distinguishes between PGCM and 3pF, which cannot be captured from  $r_{2,\psi}$  and  $R(-\eta, \eta)$ . As has been shown in Fig.5a and Fig.6a, the longitudinal decorrelation functions are almost linear in the range of  $\eta < 2$ , especially around mid-rapidity such that they can be parameterized as follows [61, 67]:

$$r_{2,V}(\eta) = 1 - 2\eta F_{2,V}(\eta), \quad (5)$$

$$r_{2,\psi}(\eta) = 1 - 2\eta F_{2,\Psi}(\eta), \quad (6)$$

where  $F_{2,V}(\eta)$  and  $F_{2,\Psi}(\eta)$  are called slope parameters.

ATLAS Collaboration suggested that these slope parameters can be measured by performing the  $\eta$ -weighted average for the deviation of correlation functions  $r_{2,V}$  and

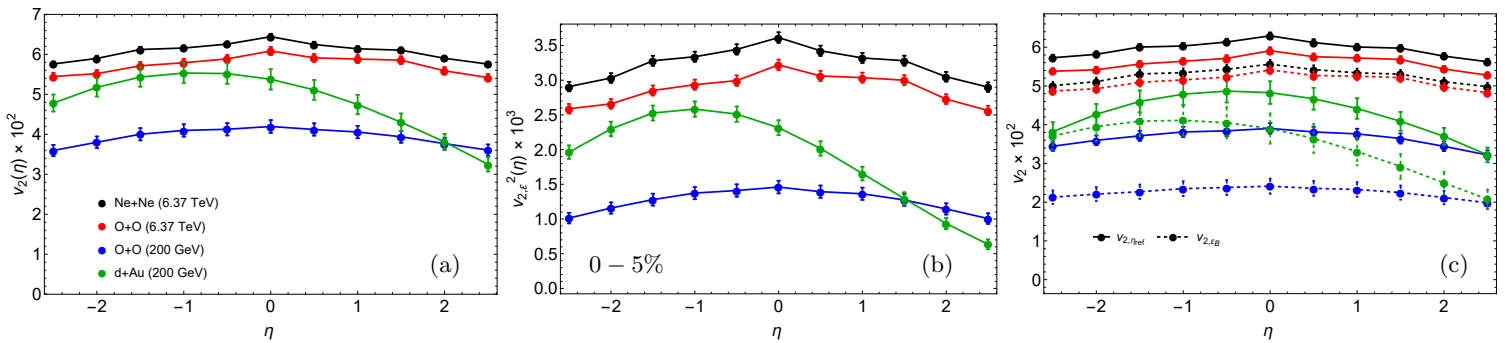


FIG. 8. Diagonal terms of 2-dimensional flow distribution  $v_2(\eta)$  are depicted in panel (a) for Ne+Ne (black), O+O (red and blue), and d+Au (green) collisions in 0 – 5% centrality, similar to Fig.3a. NLEFT configurations are considered for  $^{20}\text{Ne}$  and  $^{16}\text{O}$ . Calculations of elliptic flow projected to  $\mathcal{E}_2$  squared are presented in (b). Panel (c) shows the comparison between Eqs.9 and 10.

$r_{2;\psi}$  from the unity [78]:

$$F_{2;\psi}(\eta) = \frac{\sum_i \{1 - r_{2;\psi}(\eta_i)\} \eta_i}{2 \sum_i \eta_i^2}. \quad (7)$$

Here, we use these parameters to distinguish between different oxygen structures. These observables can be applied on experimental data to find the right nuclear structure and model. Figs.5 and 6 indicate Eq.7 is a suitable discriminator for nuclear structures. Discriminator  $F_{2;\psi}$  is not able to differentiate between NLEFT and 3pF, as well as PGCM and VMC. However, the orientation discriminator presents distinct values for all discussed models, and thus different nuclear structures can be quantified by employing this observable.

## B. Small Systems at RHIC and LHC Collisions

As mentioned in Sec.II, longitudinal initial fluctuations are encoded in decorrelation flow observables. These observables have been studied for different sizes and collision energies [51, 79, 80]. Here, we do this study for d+Au (200 GeV), O+O (200 GeV and 6.37 TeV), and Ne+Ne (6.37 TeV) collisions. We should mention that here we generate Ne+Ne and O+O collisions concerning NLEFT model. This study can give us an insight of longitudinal decorrelation in light nuclei. Fig.8a shows a comparison of elliptic flow at different  $\eta$  bins obtained by 2PC method for various systems. Concerning  $v_2(\eta)$ , identifying of different structures is accessible. As illustrated, we find:

$$\begin{aligned} v_2^{Ne+Ne} &> v_2^{O+O(L)} > v_2^{d+Au} > v_2^{O+O(R)} & \text{for } \eta < 2, \\ v_2^{Ne+Ne} &> v_2^{O+O(L)} > v_2^{O+O(R)} > v_2^{d+Au} & \text{for } \eta > 2, \end{aligned}$$

where  $L$  and  $R$  indicate the  $O + O$  collisions at LHC (6.37 TeV) and RHIC (200 GeV) energies. The results indicate the slope of  $v_2(\eta)$  is large in RHIC energies far from mid-rapidity. Also, the asymmetry of d+Au collision is manifested in this observable [81].

Using correlations between  $V_2$  and different estimates of  $\mathcal{E}_2$ , we can identify sources of initial-state-driven decorrelations contributing to  $V_{2\Delta}(\eta_a, \eta_b)$  [51, 82]. The projection of flow along the direction of eccentricity vectors at mid-rapidity is calculated by [50]:

$$v_{2,\varepsilon} \equiv \frac{\langle V_2(\eta) \mathcal{E}_2^* \rangle}{\sqrt{\langle \mathcal{E}_2 \mathcal{E}_2^* \rangle}}, \quad (8)$$

where  $\langle \dots \rangle$  indicates an average over events in specific centrality range. The main mission of this correlator is to make an observable without non-flow effect and capture the initial-state-driven short- and long-range correlations according to participant types (nucleons or quarks) [82]. Here we would like to employ  $v_{2,\varepsilon}$  to approximate the decorrelation. Fig.8b shows that Eq.8 can also reproduce the behavior of  $v_2(\eta)$ , as shown in panel (a), such that we find  $v_2(\eta)/v_{2,\varepsilon}^2(\eta)$  approximately as 1.85 for Ne+Ne, 1.95 for O+O(L), 3.1 for O+O(R), and 2.2 ( $\eta < 0.5$ ) for d+Au collision. Removing non-flow effect using  $v_{2,\varepsilon}$  leads to a non-constant ratio  $v_2(\eta)/v_{2,\varepsilon}^2(\eta)$  for d+Au collisions for the phase space  $\eta \geq 0.5$ . However, decorrelations tend to be strong in  $|\eta| > 0.5$  for all types of collisions. Furthermore, in d+Au collision there exists a shift. However, the effect of the asymmetry in this collision still exist.

The decorrelation of flow vector is derived by the difference between  $\mathcal{E}_{2,F}$  and  $\mathcal{E}_{2,B}$ . This means that flow decorrelation can be estimated by its projection along  $\mathcal{E}_{2,B}$  [50, 51]:

$$v_{2,\varepsilon_B} \equiv \frac{\langle V_2(\eta) \mathcal{E}_{2,B}^* \rangle}{\sqrt{\langle \mathcal{E}_{2,B} \mathcal{E}_{2,B}^* \rangle}}. \quad (9)$$

Notice that  $\mathcal{E}_{2,B}$  is obtained for  $-3 \leq \eta_B \leq -5$  at far-backward. To resemble this estimation, we employ the 2-point correlation for  $-3.5 \leq \eta_{ref} \leq -4.5$ :

$$v_{2,\eta_{ref}} \equiv \frac{V_{2\Delta}(\eta, \eta_{ref})}{\sqrt{v_2(\eta_{ref})}}. \quad (10)$$

Fig.8c presents a comparison of the results of Eq.9 with Eq.10 for different system collisions. It indicates  $v_{2,\eta_{ref}} >$

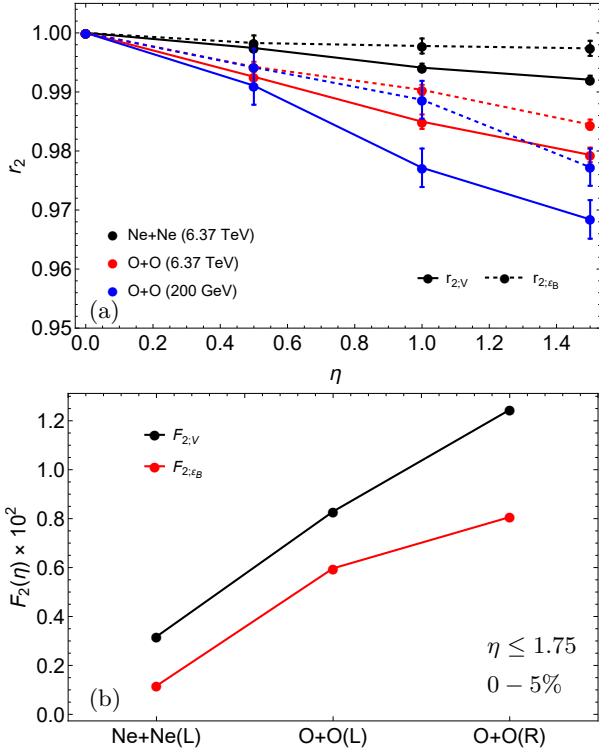


FIG. 9. (a) Correlator  $r_{2,V}$  and its estimator  $r_{2;\epsilon_B}$  are obtained for symmetric collisions, Ne+Ne and O+O, at 0 – 5% centrality. (b) To determine the rate of resembling of flow decorrelations the values of slope parameters  $F_{2,V}$  (black) and  $F_{2;\epsilon_B}$  (red) have been shown.

$v_{2,\epsilon_B}$  such that the ratio  $v_{2,\eta_{ref}}/v_{2,\epsilon_B}$  is equal to 1.3 for Ne+Ne, 1.1 for O+O(L) and 1.6 for O+O(R). This ratio is obtained 1.12 for  $\eta < 0$  and 1.3 for  $\eta \geq 0$  in d+Au collisions. These results indicate that the correlator  $v_{2,\eta_{ref}}$  approximately washes out the effect of asymmetry of the collisions, while  $v_{2,\epsilon_B}$  preserves it.

To avoid asymmetric collision effects and decrease non-flow contributions, we study the correlator  $r_{2,V} = v_{2,\eta_{ref}}(\eta)/v_{2,\eta_{ref}}(-\eta)$  and its estimator,  $r_{2;\epsilon_B} = v_{2,\epsilon_B}(\eta)/v_{2,\epsilon_B}(-\eta)$ , for the symmetric collisions. The results in 0 – 5% centrality are displayed in Fig.9a. It worths mentioning that the correlators are shown up to  $\eta = 1.75$  where they are almost linear. This enables us to investigate slope parameter for different collisions. As expected, the trends of Fig.8 also exist here such that we have  $r_2^{Ne+Ne} > r_2^{O+O(L)} > r_2^{O+O(R)}$ , although the difference between  $r_2^{O+O(L)}$  and  $r_2^{O+O(R)}$  is decreased concerning the projection of flow vector on  $\mathcal{E}_B$ . Nonetheless, this projection decreases the decorrelations as depicted in Fig.8c. This results are consistent with the trends in Ref.[37]. It means that this tendency is also preserved in small systems and can be studied by employing slope parameter Eq.7 as depicted in Fig.9b. The difference between collisions are extracted using  $F_2(\eta)$ . It is observed that  $F_{2;\epsilon_B} < F_{2,V}$  and  $F_2^{Ne+Ne} < F_2^{O+O(L)} < F_2^{O+O(R)}$ .

However, this observable shows the decorrelations are decreased in Ne+Ne collisions more significantly than O+O collisions. The ratio  $F_{2;\epsilon_B}/F_{2,V}$  gives the rate of resembling of flow decorrelation slope. It is  $\approx 37\%$  for Ne+Ne,  $\approx 72\%$  for O+O(L) and  $\approx 65\%$  for O+O(R). Since the results of  $r_2$  in Fig.9a are not perfectly linear, we fit the right hand side of Eq.5 ( $1 - 2\eta F_2$ ) to  $r_2$ . Fitting shows minor differences in the ratio of  $F_{2;\epsilon_B}/F_{2,V}$  as  $\approx 41\%$  for Ne+Ne,  $\approx 72\%$  for O+O(L) and  $\approx 61\%$  for O+O(R).

Estimation of elliptic flow angle decorrelation between two bins centered at  $\eta$  and  $-\eta$  is defined [57, 83]:

$$\langle \cos(2\psi_2(\eta) - 2\psi_2(-\eta)) \rangle = \left\langle \frac{V_2(\eta)V_2^*(-\eta)}{|V_n(\eta)||V_n(-\eta)|} \right\rangle. \quad (11)$$

Unlike  $V_{2\Delta}(\eta, -\eta)$ , flow angle decorrelation can be measured experimentally. However, since the flow angle decorrelation is largest if the magnitude of overall flow is small, scatter plot of  $\cos(2\Delta\psi_2)$  and overall flow magnitude gives us a useful information about higher moments of the overall flow magnitude [83]. Moreover, it can be shown that the decorrelations is smaller in higher moments. In this way, we study how this inverse relation between  $\cos(2\Delta\psi)$  and  $v_2$  would be for different system collisions. The scattered plots are displayed in Fig.10. Different collisions can be understood from the distributions in this figure such that flow angle fluctuates for d+Au in a wider range than other collisions. The most flow angle fluctuations in Ne+Ne and O+O collisions occur while  $v_2$  is close to zero. This pattern is unlike what happens in large systems [57]. Ref.[57] shows that an increase in  $\cos(2\Delta\psi)$  leads to a decrease in overall flow magnitude  $v_2$  in the context of a random model. The anticorrelation of the flow angle decorrelation  $\Delta\psi_2$  with  $v_2$  is depicted as the red points in Fig.10. We note that the relation between flow angle decorrelation and overall flow magnitude tells us more details about the collision energies as well as type of systems and it can be concluded using this anticorrelation.

#### IV. CONCLUSION

In this study, we conducted a comprehensive analysis of longitudinal flow decorrelations in light ion collisions at both RHIC and LHC energies. Our investigation focused on flow decorrelations across various advanced *ab-initio* models of oxygen structure, as well as the spherical oxygen charge density (3pF) at 200 GeV. Notably, we identified that the correlator  $V_{2\Delta}$  effectively differentiates the VMC structure from NLEFT and PGCM, revealing similar behaviors between NLEFT and PGCM. This distinction was clearly demonstrated through the ratio  $v_2(\eta)_{\text{configs}}/v_2(\eta)_{3\text{pF}}$ .

Furthermore, we captured the deformation of different structures by subtracting the flow decorrelations of configurations from 3pF (independent nucleons) observables. A significant negative contribution was observed for VMC when compared to NLEFT and PGCM. The

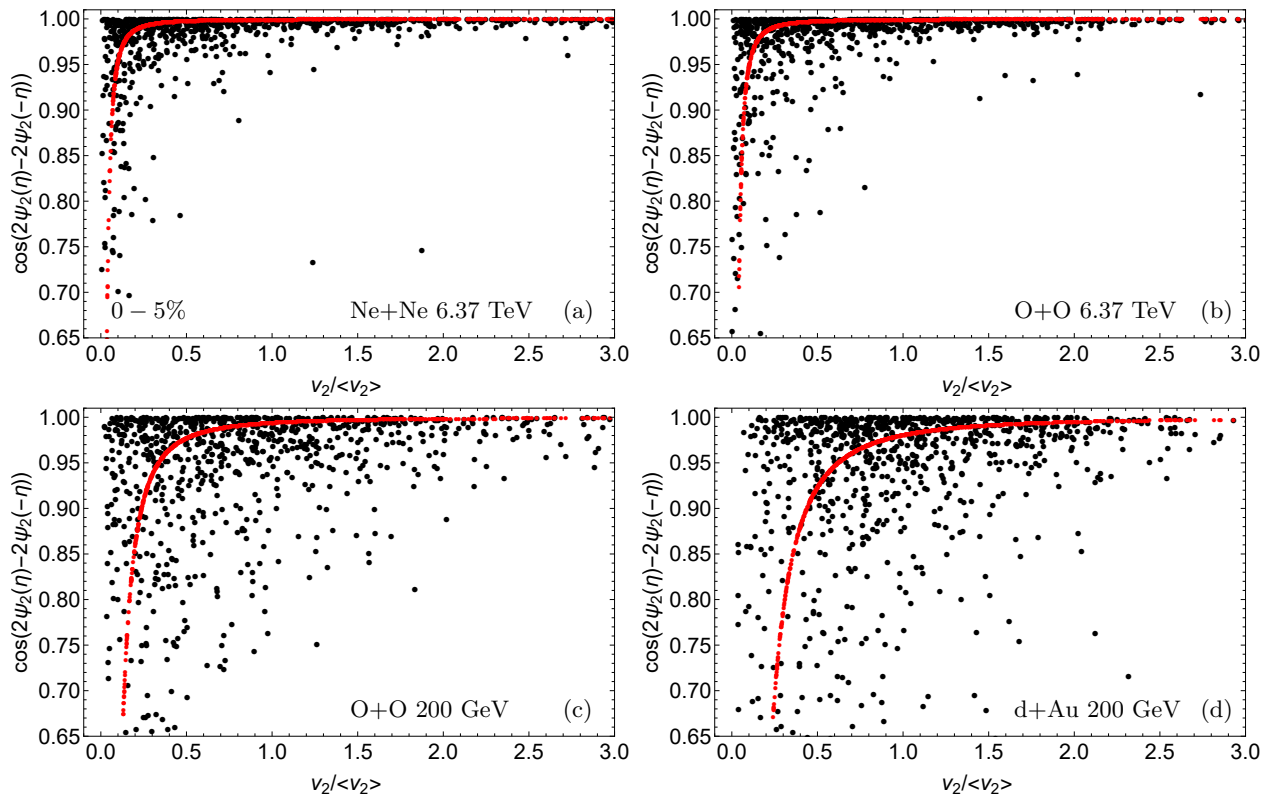


FIG. 10. Scattered plot of  $\cos(2\psi_2(\eta) - 2\psi_2(-\eta))$  angle decorrelation versus the elliptic flow magnitude for the hydrodynamic model, for Ne+Ne (a), O+O(L) (b), O+O(R) (c) and d+Au (d) collisions at 0 – 5% centrality. The pseudorapidity bin  $\eta = 2$  is considered here. The expected flow angle decorrelation as function of the fixed value of flow are presented by red points.

correlator  $R(-\eta, \eta)$  enhanced the resolution of discrimination, achieving a separation between NLEFT and PGCM of up to 2%. However, the distinction between VMC and other configurations remained robust.

Utilizing  $r_2$  to mitigate non-flow effects proved beneficial in identifying various modeled structures. Our results indicated that  $r_{2;V}$  effectively discriminated NLEFT from other configurations, while  $r_{2;\psi}$  distinguished VMC from alternative structures. Additionally,  $r_{2;V}$  was successful in separating PGCM from the spherical oxygen structure. We also derived slope parameters as suggested by ATLAS for different configurations, highlighting that the slope parameter  $F_{2;\psi}$  serves as a suitable discriminator for nuclear structures.

To facilitate comparisons across systems at RHIC and LHC energies, we examined flow decorrelations for d+Au and O+O collisions at 200 GeV, as well as Ne+Ne and O+O for upcoming LHC runs at 6.37 TeV. Our findings revealed a hierarchy in decorrelations across different systems, specifically  $v_2^{Ne+Ne} > v_2^{O+O(L)} > v_2^{d+Au} > v_2^{O+O(R)}$ . We also observed the impact of asymmetry in d+Au collisions; although this effect was mitigated by the correlator  $V_{2\Delta}(\eta, \eta_{ref})$ , it could be restored through

correlations of flow with the initial source in the backward  $\mathcal{E}_B$  (or forward  $\mathcal{E}_F$ ) pseudorapidity bin.

We noted a decrease in  $v_{2,\mathcal{E}_B}$ , which contributed to the reduction of non-flow effects in the  $r_2$  correlator. This reduction was corroborated by our observations of slope parameters, which reflected the extent of flow decorrelations across different systems. Additionally, our analysis of flow angle decorrelations revealed diverse distributions in scatter plots of  $\cos(2\Delta\psi)$  versus overall flow magnitude, with flow angles exhibiting greater fluctuations in d+Au collisions compared to others. Finally, we measured the mean values of these correlations using a random model, indicating that the most significant angle fluctuations for Ne+Ne and O+O at LHC energy occur when the overall flow magnitude approaches zero.

## ACKNOWLEDGMENTS

We thanks Huichao Song and Jiangyong Jia for insightful discussions. We are grateful to the participants of the 4th international workshop on QCD collectivity at the smallest scales for useful conversations. This work is supported in part by the National Natural Science Foundation of China under Grant No. 12247107.



- [1] F. Close, “Nuclear Physics: A Very Short Introduction,” Oxford University Press, D 2015, 8 23 Jul 2015.
- [2] J. P. Delaroche, M. Girod, J. Libert, H. Goutte, S. Hilaire, S. Peru, N. Pillet and G. F. Bertsch, “Structure of even-even nuclei using a mapped collective Hamiltonian and the D1S Gogny interaction,” *Phys. Rev. C* **81** (2010), 014303
- [3] P. Y. Wang, J. G. Li, S. Zhang, Q. Yuan, M. R. Xie and W. Zuo, “Ab initio calculations with a new local chiral N3LO nucleon-nucleon force,” *Phys. Rev. C* **109** (2024) no.6, 064316
- [4] A. Demyanova, A. Danilov, V. Starastin, S. Goncharov and T. Leonova, “Search for states with enhanced radii in  $^{20}\text{Ne}$ ,” *AIP Conf. Proc.* **3020** (2024) no.1, 020001
- [5] S. Hamada, A. H. Al-Ghamdi, A. A. Alholaisi, A. A. Ibraheem, N. Amangeldi and Y. Abdou, “Analysis of elastic scattering of  $6,7\text{Li}$  and  $20\text{Ne}$  from  $24\text{Mg}$  nucleus using microscopic potentials,” *Int. J. Mod. Phys. E* **32** (2023) no.03n04, 235001
- [6] L. Morales-Gallegos, M. Aliotta, A. Best, C. G. Bruno, R. Buompane, T. Davinson, M. D. Cesare, A. D. Leva, A. D’Onofrio and J. G. Duarte, *et al.* “Direct measurements of the  $12\text{C}(12\text{C},p)23\text{Na}$  and  $12\text{C}(12\text{C},\alpha)20\text{Ne}$  reactions at low energies for Nuclear Astrophysics,” *EPJ Web Conf.* **260** (2022), 01006
- [7] D. Kekejian, “Deformed No-Core Shell Model and Symplectic Effective Field Theory,” doi:10.31390/gradschool\_dissertations.5748
- [8] X. F. Yang, S. J. Wang, S. G. Wilkins and R. F. Garcia Ruiz, “Laser spectroscopy for the study of exotic nuclei,” *Prog. Part. Nucl. Phys.* **129** (2023), 104005
- [9] N. Magdy, M. Hegazy, A. Rafaat, W. Li, A. Deshpande, A. M. H. Abdelhady, A. Y. Ellithi, R. A. Lacey and Z. Tu, “A study of nuclear structure of light nuclei at the electron-ion collider,” *Eur. Phys. J. A* **60** (2024) no.10, 212
- [10] D. Cline, “Nuclear shapes studied by coulomb excitation,” *Ann. Rev. Nucl. Part. Sci.* **36** (1986), 683-716
- [11] U. G. Meißner, “A new tool in nuclear physics: Nuclear lattice simulations,” *Nucl. Phys. News.* **24** (2014) no.4, 11-15
- [12] S. Elhatisari, E. Epelbaum, H. Krebs, T. A. Lähde, D. Lee, N. Li, B. n. Lu, U. G. Meißner and G. Rupak, “Ab initio Calculations of the Isotopic Dependence of Nuclear Clustering,” *Phys. Rev. Lett.* **119** (2017) no.22, 222505
- [13] M. Frosini, T. Duguet, J. P. Ebran and V. Somà, “Multi-reference many-body perturbation theory for nuclei: I. Novel PGCM-PT formalism,” *Eur. Phys. J. A* **58** (2022) no.4, 62
- [14] M. Frosini, T. Duguet, J. P. Ebran, B. Bally, T. Mongelli, T. R. Rodríguez, R. Roth and V. Somà, “Multi-reference many-body perturbation theory for nuclei: II. Ab initio study of neon isotopes via PGCM and IM-NCSM calculations,” *Eur. Phys. J. A* **58** (2022) no.4, 63
- [15] M. Frosini, T. Duguet, J. P. Ebran, B. Bally, H. Hergert, T. R. Rodríguez, R. Roth, J. Yao and V. Somà, “Multi-reference many-body perturbation theory for nuclei: III. Ab initio calculations at second order in PGCM-PT,” *Eur. Phys. J. A* **58** (2022) no.4, 64
- [16] D. Lonardonì, S. Gandolfi, J. E. Lynn, C. Petrie, J. Carlson, K. E. Schmidt and A. Schwenk, “Auxiliary field diffusion Monte Carlo calculations of light and medium-mass nuclei with local chiral interactions,” *Phys. Rev. C* **97** (2018) no.4, 044318
- [17] J. Jia, G. Giacalone, B. Bally, J. D. Brandenburg, U. Heinz, S. Huang, D. Lee, Y. J. Lee, C. Loizides and W. Li, *et al.* “Imaging the initial condition of heavy-ion collisions and nuclear structure across the nuclide chart,” *Nucl. Sci. Tech.* **35** (2024) no.12, 220
- [18] M. I. Abdulhamid *et al.* [STAR], “Imaging shapes of atomic nuclei in high-energy nuclear collisions,” *Nature* **635** (2024) no.8037, 67-72
- [19] G. Giacalone, “Many-body correlations for nuclear physics across scales: from nuclei to quark-gluon plasmas to hadron distributions,” *Eur. Phys. J. A* **59** (2023) no.12, 297
- [20] J. Y. Ollitrault, “Measures of azimuthal anisotropy in high-energy collisions,” *Eur. Phys. J. A* **59** (2023) no.10, 236
- [21] B. Alver and G. Roland, “Collision geometry fluctuations and triangular flow in heavy-ion collisions,” *Phys. Rev. C* **81** (2010), 054905
- [22] M. A. Stephanov, K. Rajagopal and E. V. Shuryak, “Event-by-event fluctuations in heavy ion collisions and the QCD critical point,” *Phys. Rev. D* **60** (1999), 114028
- [23] C. E. Aguiar, Y. Hama, T. Kodama and T. Osada, “Event-by-event fluctuations in hydrodynamical description of heavy ion collisions,” *Nucl. Phys. A* **698** (2002), 639-642
- [24] P. Huovinen and P. V. Ruuskanen, “Hydrodynamic Models for Heavy Ion Collisions,” *Ann. Rev. Nucl. Part. Sci.* **56** (2006), 163-206
- [25] S. A. Voloshin, A. M. Poskanzer and R. Snellings, “Collective phenomena in non-central nuclear collisions,” *Landolt-Bornstein* **23** (2010), 293-333
- [26] U. Heinz and R. Snellings, “Collective flow and viscosity in relativistic heavy-ion collisions,” *Ann. Rev. Nucl. Part. Sci.* **63** (2013), 123-151
- [27] J. Jia, “Probing triaxial deformation of atomic nuclei in high-energy heavy ion collisions,” *Phys. Rev. C* **105** (2022) no.4, 044905
- [28] J. Jia, “Shape of atomic nuclei in heavy ion collisions,” *Phys. Rev. C* **105** (2022) no.1, 014905
- [29] N. M. Fortier, S. Jeon and C. Gale, “Heavy-ion collisions as probes of nuclear structure,” *Phys. Rev. C* **111** (2025) no.1, L011901
- [30] B. Bally, M. Bender, G. Giacalone and V. Somà, “Evidence of the triaxial structure of  $^{129}\text{Xe}$  at the Large Hadron Collider,” *Phys. Rev. Lett.* **128** (2022) no.8, 082301
- [31] C. Zhang and J. Jia, “Evidence of Quadrupole and Octupole Deformations in  $\text{Zr}96+\text{Zr}96$  and  $\text{Ru}96+\text{Ru}96$  Collisions at Ultrarelativistic Energies,” *Phys. Rev. Lett.* **128** (2022) no.2, 022301
- [32] G. Giacalone, J. Jia and C. Zhang, “Impact of Nuclear Deformation on Relativistic Heavy-Ion Collisions: Assessing Consistency in Nuclear Physics across Energy Scales,” *Phys. Rev. Lett.* **127** (2021) no.24, 242301
- [33] G. Nijs and W. van der Schee, “Inferring nuclear structure from heavy isobar collisions using Trajectum,” *SciPost Phys.* **15** (2023) no.2, 041
- [34] J. Jia, G. Giacalone and C. Zhang, “Separating the Impact of Nuclear Skin and Nuclear Deformation in High-

- Energy Isobar Collisions,” *Phys. Rev. Lett.* **131** (2023) no.2, 022301
- [35] N. Summerfield, B. N. Lu, C. Plumberg, D. Lee, J. Noronha-Hostler and A. Timmins, “ $^{16}\text{O}$   $^{16}\text{O}$  collisions at energies available at the BNL Relativistic Heavy Ion Collider and at the CERN Large Hadron Collider comparing  $\alpha$  clustering versus substructure,” *Phys. Rev. C* **104** (2021) no.4, L041901
- [36] S. Huang, “Measurements of azimuthal anisotropies in  $^{16}\text{O}+^{16}\text{O}$  and  $\gamma$ +Au collisions from STAR,” [arXiv:2312.12167 [nucl-ex]].
- [37] C. Zhang, J. Chen, G. Giacalone, S. Huang, J. Jia and Y. G. Ma, “*Ab-initio* nucleon-nucleon correlations and their impact on high energy  $^{16}\text{O}+^{16}\text{O}$  collisions,” [arXiv:2404.08385 [nucl-th]].
- [38] Y. Wang, S. Zhao, B. Cao, H. j. Xu and H. Song, “Exploring the compactness of  $\alpha$  clusters in O16 nuclei with relativistic O16+O16 collisions,” *Phys. Rev. C* **109** (2024) no.5, L051904
- [39] S. Prasad, N. Mallick, R. Sahoo and G. G. Barnaföldi, “Anisotropic flow fluctuation as a possible signature of clustered nuclear geometry in O–O collisions at the Large Hadron Collider,” *Phys. Lett. B* **860** (2025), 139145
- [40] G. Giacalone, B. Bally, G. Nijs, S. Shen, T. Duguet, J. P. Ebran, S. Elhatisari, M. Frosini, T. A. Lähde and D. Lee, *et al.* “The unexpected uses of a bowling pin: exploiting  $^{20}\text{Ne}$  isotopes for precision characterizations of collectivity in small systems,” [arXiv:2402.05995 [nucl-th]].
- [41] G. Giacalone, W. Zhao, B. Bally, S. Shen, T. Duguet, J. P. Ebran, S. Elhatisari, M. Frosini, T. A. Lähde and D. Lee, *et al.* “The unexpected uses of a bowling pin: anisotropic flow in fixed-target  $^{208}\text{Pb}+^{20}\text{Ne}$  collisions as a probe of quark-gluon plasma,” [arXiv:2405.20210 [nucl-th]].
- [42] P. Bozek, W. Broniowski and J. Moreira, “Torqued fireballs in relativistic heavy-ion collisions,” *Phys. Rev. C* **83** (2011), 034911
- [43] W. Broniowski, P. Bozek and J. Moreira, “Forward-backward flow correlations in relativistic heavy-ion collisions,” *Prog. Theor. Phys. Suppl.* **193** (2012), 323-326
- [44] P. Bozek, A. Bzdak and G. L. Ma, “Rapidity dependence of elliptic and triangular flow in proton–nucleus collisions from collective dynamics,” *Phys. Lett. B* **748** (2015), 301-305
- [45] P. Bozek and W. Broniowski, “The torque effect and fluctuations of entropy deposition in rapidity in ultra-relativistic nuclear collisions,” *Phys. Lett. B* **752** (2016), 206-211
- [46] A. Bzdak and P. Bozek, “Multiparticle long-range rapidity correlations from fluctuation of the fireball longitudinal shape,” *Phys. Rev. C* **93** (2016) no.2, 024903
- [47] P. Bozek, “Principal component analysis of the nonlinear coupling of harmonic modes in heavy-ion collisions,” *Phys. Rev. C* **97** (2018) no.3, 034905
- [48] P. Bozek, “Interplay of longitudinal and transverse expansion in the kinetic dynamics of heavy-ion collisions,” *Phys. Rev. C* **107** (2023) no.3, 034916
- [49] K. Xiao, F. Liu and F. Wang, “Event-plane decorrelation over pseudorapidity and its effect on azimuthal anisotropy measurements in relativistic heavy-ion collisions,” *Phys. Rev. C* **87** (2013) no.1, 011901
- [50] J. Jia and P. Huo, “Forward-backward eccentricity and participant-plane angle fluctuations and their influences on longitudinal dynamics of collective flow,” *Phys. Rev. C* **90** (2014) no.3, 034915
- [51] C. Zhang, S. Huang and J. Jia, “Longitudinal Structure of Quark-Gluon Plasma Unveiled Through Nuclear Deformations,” [arXiv:2405.08749 [nucl-th]].
- [52] S. Voloshin and Y. Zhang, “Flow study in relativistic nuclear collisions by Fourier expansion of Azimuthal particle distributions,” *Z. Phys. C* **70** (1996), 665-672
- [53] M. Luzum and H. Petersen, “Initial State Fluctuations and Final State Correlations in Relativistic Heavy-Ion Collisions,” *J. Phys. G* **41** (2014), 063102
- [54] G. Aad *et al.* [ATLAS], “Measurement of the azimuthal anisotropy for charged particle production in  $\sqrt{s_{NN}} = 2.76$  TeV lead-lead collisions with the ATLAS detector,” *Phys. Rev. C* **86** (2012), 014907
- [55] H. Mehrabpour and S. F. Taghavi, “Non-Bessel–Gaussianity and flow harmonic fine-splitting,” *Eur. Phys. J. C* **79** (2019) no.1, 88
- [56] A. Bilandzic, R. Snellings and S. Voloshin, “Flow analysis with cumulants: Direct calculations,” *Phys. Rev. C* **83** (2011), 044913
- [57] P. Bozek and H. Mehrabpour, “Random model of flow decorrelation,” *Phys. Rev. C* **108** (2023) no.2, 024907
- [58] P. Bozek, W. Broniowski and A. Olszewski, “Two-particle correlations in pseudorapidity in a hydrodynamic model,” *Phys. Rev. C* **92** (2015) no.5, 054913
- [59] F. G. Gardim, F. Grassi, M. Luzum and J. Y. Ollitrault, “Breaking of factorization of two-particle correlations in hydrodynamics,” *Phys. Rev. C* **87** (2013) no.3, 031901
- [60] V. Khachatryan *et al.* [CMS], “Evidence for transverse momentum and pseudorapidity dependent event plane fluctuations in PbPb and pPb collisions,” *Phys. Rev. C* **92** (2015) no.3, 034911
- [61] M. Aaboud *et al.* [ATLAS], “Measurement of longitudinal flow decorrelations in Pb+Pb collisions at  $\sqrt{s_{NN}} = 2.76$  and 5.02 TeV with the ATLAS detector,” *Eur. Phys. J. C* **78** (2018) no.2, 142
- [62] S. Chatrchyan *et al.* [CMS], “Studies of Azimuthal Dihadron Correlations in Ultra-Central PbPb Collisions at  $\sqrt{s_{NN}} = 2.76$  TeV,” *JHEP* **02** (2014), 088
- [63] Y. Zhou [ALICE], “Searches for  $p_T$  dependent fluctuations of flow angle and magnitude in Pb-Pb and p-Pb collisions,” *Nucl. Phys. A* **931** (2014), 949-953
- [64] P. Huo [ATLAS], “Measurement of longitudinal flow correlations in Pb+Pb collisions at  $\sqrt{s_{NN}} = 2.76$  and 5.02 TeV with the ATLAS detector,” *Nucl. Phys. A* **967** (2017), 908-911
- [65] P. Bożek, W. Broniowski and A. Olszewski, “Hydrodynamic modeling of pseudorapidity flow correlations in relativistic heavy-ion collisions and the torque effect,” *Phys. Rev. C* **91** (2015), 054912
- [66] K. Xiao, L. Yi, F. Liu and F. Wang, “Factorization of event-plane correlations over transverse momentum in relativistic heavy ion collisions in a multiphase transport model,” *Phys. Rev. C* **94** (2016) no.2, 024905
- [67] J. Jia, P. Huo, G. Ma and M. Nie, “Observables for longitudinal flow correlations in heavy-ion collisions,” *J. Phys. G* **44** (2017) no.7, 075106
- [68] P. Bożek, “Angle and magnitude decorrelation in the factorization breaking of collective flow,” *Phys. Rev. C* **98** (2018) no.6, 064906
- [69] C. Shen and B. Schenke, “Dynamical initial state model for relativistic heavy-ion collisions,” *Phys. Rev. C* **97** (2018) no.2, 024907

- [70] B. Schenke, S. Jeon and C. Gale, “Elliptic and triangular flow in event-by-event (3+1)D viscous hydrodynamics,” *Phys. Rev. Lett.* **106** (2011), 042301
- [71] B. Schenke, S. Jeon and C. Gale, “(3+1)D hydrodynamic simulation of relativistic heavy-ion collisions,” *Phys. Rev. C* **82** (2010), 014903
- [72] X. L. Zhao, G. L. Ma, Y. Zhou, Z. W. Lin and C. Zhang, “Nuclear cluster structure effect in  $^{16}\text{O}+^{16}\text{O}$  collisions at the top RHIC energy,” [arXiv:2404.09780 [nucl-th]].
- [73] J. Takahashi, B. M. Tavares, W. L. Qian, R. Andrade, F. Grassi, Y. Hama, T. Kodama and N. Xu, “Topology studies of hydrodynamics using two particle correlation analysis,” *Phys. Rev. Lett.* **103** (2009), 242301
- [74] P. Filip, R. Lednicky, H. Masui and N. Xu, “Initial eccentricity in deformed Au-197 + Au-197 and U-238 + U-238 collisions at sNN=200 GeV at the BNL Relativistic Heavy Ion Collider,” *Phys. Rev. C* **80** (2009), 054903
- [75] Q. Y. Shou, Y. G. Ma, P. Sorensen, A. H. Tang, F. Videbæk and H. Wang, “Parameterization of Deformed Nuclei for Glauber Modeling in Relativistic Heavy Ion Collisions,” *Phys. Lett. B* **749** (2015), 215-220
- [76] L. Adamczyk *et al.* [STAR], “Azimuthal anisotropy in U+U and Au+Au collisions at RHIC,” *Phys. Rev. Lett.* **115** (2015) no.22, 222301
- [77] M. Nie, C. Zhang, Z. Chen, L. Yi and J. Jia, “Impact of nuclear structure on longitudinal flow decorrelations in high-energy isobar collisions,” *Phys. Lett. B* **845** (2023), 138177
- [78] X. Y. Wu, L. G. Pang, G. Y. Qin and X. N. Wang, “Longitudinal fluctuations and decorrelations of anisotropic flows at energies available at the CERN Large Hadron Collider and at the BNL Relativistic Heavy Ion Collider,” *Phys. Rev. C* **98** (2018) no.2, 024913
- [79] P. Bozek and W. Broniowski, “Elliptic Flow in Ultrarelativistic Collisions with Polarized Deuterons,” *Phys. Rev. Lett.* **121** (2018) no.20, 202301
- [80] X. Y. Wu and G. Y. Qin, “Asymmetric longitudinal flow decorrelations in proton-nucleus collisions,” [arXiv:2109.03512 [hep-ph]].
- [81] C. Shen, J. F. Paquet, G. S. Denicol, S. Jeon and C. Gale, “Collectivity and electromagnetic radiation in small systems,” *Phys. Rev. C* **95** (2017) no.1, 014906
- [82] J. Jia, S. Huang, C. Zhang and S. Bhatta, “Sources of longitudinal flow decorrelations in high-energy nuclear collisions,” [arXiv:2408.15006 [nucl-th]].
- [83] P. Bozek and W. Broniowski, “Longitudinal decorrelation measures of flow magnitude and event-plane angles in ultrarelativistic nuclear collisions,” *Phys. Rev. C* **97** (2018) no.3, 034913